

Properly ordered dimers, R -charges, and an efficient inverse algorithm

To cite this article: Daniel R. Gulotta JHEP10(2008)014

View the [article online](#) for updates and enhancements.

Related content

- [Dimer models and quiver gauge theories](#)
Ramadevi Pichai
- [A note on dimer models and D-brane gauge theories](#)
Prarit Agarwal, P. Ramadevi and Tapobrata Sarkar
- [Moduli spaces of gauge theories from Dimer models: proof of the correspondence](#)
Sebastián Franco and David Vegh

Recent citations

- [Semi-steady non-commutative crepant resolutions via regular dimer models](#)
Yusuke Nakajima
- [Non-commutative crepant resolutions of Gorenstein rings with small class group](#)
Yusuke Nakajima
- [Calabi–Yau Volumes and Reflexive Polytopes](#)
Yang-Hui He *et al*

Properly ordered dimers, R -charges, and an efficient inverse algorithm

Daniel R. Gulotta

*Department of Physics, Princeton University,
Princeton, NJ 08544, U.S.A.
E-mail: dgulotta@princeton.edu*

ABSTRACT: The $\mathcal{N} = 1$ superconformal field theories that arise in AdS-CFT from placing a stack of D3-branes at the singularity of a toric Calabi-Yau threefold can be described succinctly by dimer models. We present an efficient algorithm for constructing a dimer model from the geometry of the Calabi-Yau. Since not all dimers produce consistent field theories, we perform several consistency checks on the field theories produced by our algorithm: they have the correct number of gauge groups, their cubic anomalies agree with the Chern-Simons coefficients in the AdS dual, and all gauge invariant chiral operators satisfy the unitarity bound. We also give bounds on the ratio of the central charge of the theory to the area of the toric diagram. To prove these results, we introduce the concept of a properly ordered dimer.

KEYWORDS: Conformal Field Models in String Theory, AdS-CFT Correspondence, Gauge Symmetry, Anomalies in Field and String Theories.

Contents

1. Introduction	1
2. Definitions	2
3. Consistency of dimer field theories	4
3.1 Criteria for consistency and inconsistency	4
3.2 Some perfect matchings of properly ordered dimers	6
3.3 Zigzag paths and (p, q) -legs	7
3.4 Unique corner perfect matchings	9
3.5 R -charges and cubic anomalies	10
3.6 Unitarity bound	14
4. Bounds on a	16
4.1 Bounds on a for toric theories	16
4.2 Comparison to non-toric field theories	18
5. Merging zigzag paths	19
5.1 Deleting an edge of the dimer	19
5.2 Making multiple deletions	20
5.3 Extra crossings	20
6. An efficient inverse algorithm	22
6.1 Description of the algorithm	22
6.2 Proof of the algorithm	25
6.3 Allowing extra crossings	28
6.4 The number of independent solutions to the R -charge equations	28
7. Conclusions	29

1. Introduction

The AdS-CFT correspondence [1–3] tells us that Type IIB string theory on $AdS_5 \times X_5$, where X is a five-dimensional Sasaki-Einstein manifold, is dual to a four-dimensional $\mathcal{N} = 1$ superconformal gauge theory. We can study the gauge theory by placing D3-branes at a singularity of Y_6 , the cone over X_5 , which is a Calabi-Yau threefold.

In the case where Y_6 is toric, dimer models [4–10] are a convenient way of encoding the field content and superpotential of the CFT. One can try to compute the geometry from the dimer or vice versa. There are algorithms for solving the former problem by taking

the determinant of the Kasteleyn matrix [4–10] and by counting the windings of zigzag paths [8–10]. The latter problem can be solved by the “Fast Inverse Algorithm” [8–10], although the algorithm is computationally infeasible for all but very simple toric varieties due to the large amount of trial and error required. We resolve this problem by eliminating the need for trial and error. Our algorithm uses some ideas from the Fast Inverse Algorithm and the method of partial resolution of the toric singularity [11–14].

One difficulty in constructing dimers is that not every dimer describes a consistent field theory. One way of determining that a field theory is not consistent is by counting its faces. Each face represents a gauge group, and a consistent theory should have as many gauge groups as there are cycles for Type IIB D-branes to wrap in the AdS theory. Previously there was not a simple, easy to check criterion for determining that a dimer is consistent. We propose that any dimer that has the correct number of faces and that has no nodes of valence one is consistent. We will present several pieces of evidence to support our proposal.

If the dimer is consistent, then the cubic anomalies of the CFT should be equal to the Chern-Simons coefficients of the AdS dual [3, 15]. We show that equality holds in dimers that meet our two criteria.

In a four-dimensional SCFT the unitarity bound says that each gauge invariant scalar operator should have dimension at least one [16], and the R -charge of a chiral primary operator is two-thirds of its dimension [17]. However, when we try to compute the R -charge of a gauge invariant chiral primary operator in an inconsistent dimer theory, the answer is sometimes less than two-thirds. We will show that in dimers that meet our two criteria, the R -charges of chiral primary operators are always at least two-thirds if the number of colors is sufficiently large.

We also show that dimers that meet our two criteria have the properties that corner perfect matchings are unique, and that the zigzag path windings agree with the (p, q) -legs of the toric diagram.

While studying R -charges, we prove that $\frac{27N^2K}{8\pi^2} < a \leq \frac{N^2K}{2}$ for toric theories, where a is the cubic 't Hooft anomaly $\frac{3}{32}(3 \text{Tr } R^3 - \text{Tr } R)$, N is the number of colors of each gauge group, and K is the area of the toric diagram (which is half the number of gauge groups).

2. Definitions

A *dimer model* [4–10] consists of a graph whose vertices are colored black or white, and every edge connects a white vertex to a black vertex, i. e. the graph is bipartite. We will use dimer models embedded on the torus T^2 to describe toric quiver gauge theories.

A *perfect matching* of the dimer is a set of edges of the dimer such that each vertex is an endpoint of exactly one of the edges. The difference of two perfect matchings is the set of edges that belong to exactly one of the matchings.

The *Kasteleyn matrix* is a weighted adjacency matrix of the dimer. There is one row for each white vertex and one column for each black vertex. Let γ_w and γ_z be a pair of curves whose winding numbers generate the homology group $H^1(T^2)$. The weight of an

edge is $cw^a z^b$ where c is an arbitrary nonzero complex number,¹ w and z are variables, a is the number of times γ_w crosses the edge with the white edge endpoint on its left minus the number of times γ_w crosses the edge with the white endpoint on its right and b is defined similarly with γ_w replaced by γ_z . The determinant of this matrix tells us the geometry of the field configuration.

The *Newton polygon* of a multivariate polynomial is the convex hull of the set of exponents of monomials appearing in the polynomial. The Newton polygon of the determinant is known as the *toric diagram*. If we choose a different basis for computing the Kasteleyn matrix, then the toric diagram changes by an affine transformation.

A (p, q) -leg of a toric diagram is a line segment drawn perpendicular to and proportional in length to a segment joining consecutive boundary lattice points of the diagram.

A *zigzag path* is a path of the dimer on which edges alternate between being clockwise adjacent around a vertex and being counterclockwise adjacent around a vertex. A zigzag path is uniquely determined by a choice of an edge and whether to turn clockwise or counterclockwise to find the next edge. Therefore each edge belongs to two zigzag paths. (These paths could turn out to be the same, although it will turn out that we want to work with models in which they are always different.)

In [8] it is conjectured that in a consistent field theory, the toric diagram can also be computed by looking at the windings of the zigzag paths: they are in one-to-one correspondence with the (p, q) -legs. The conjecture was proved using mirror symmetry in [9].

The *unsigned crossing number* of a pair of closed paths on the torus is the number of times they intersect. The *signed crossing number* of a pair of oriented closed paths on the torus is the number of times they intersect with a positive orientation (the tangent vector to the second path is counterclockwise from the tangent to the first at the point of intersection) minus the number of times they intersect with a negative orientation. It is a basic fact from homology theory that the signed crossing number of a path with winding (a, b) and a path with winding (c, d) is $(a, b) \wedge (c, d) = ad - bc$.

We will work with the zigzag path diagrams of [8] (referred to there as rhombus loop diagrams). We obtain a zigzag path diagram from a dimer as follows. For each edge of the dimer we draw a vertex of the zigzag path diagram at a point on that edge. To avoid confusion between the vertices of this diagram and the vertices of the dimer we will call the latter nodes. We connect two vertices of the zigzag path diagram if the dimer edges they represent are consecutive along a zigzag path. (This is equivalent to them being consecutive around a node and also to them being consecutive around a face.) We orient the edges of the zigzag path diagram as follows. If the endpoints lie on dimer edges that meet at a white (resp. black) node, then the edge should go counterclockwise (resp. clockwise) as seen from that node. With this definition, each node of the dimer becomes a face of the zigzag path diagram, with all edges oriented counterclockwise for a white node, or clockwise for a black node. The other faces of the zigzag path diagram correspond to faces of the dimer, and

¹The original definition of the Kasteleyn matrix imposes constraints on c for the purpose of counting perfect matchings [5–8]. However, these constraints are not necessary for determining the Newton polygon. We follow the convention of [9], which points out that it is useful for the purposes of mirror symmetry to allow arbitrary nonzero coefficients.

the orientations of their edges alternate. Figure 17 shows an example of a dimer and its corresponding zigzag path diagram.

Conversely, we can obtain a dimer from a zigzag path diagram provided that the orientations of the intersections alternate along each path. Around each vertex of such a zigzag path diagram, there is one face with all counterclockwise oriented edges, one face with all clockwise oriented edges, and two faces whose edge orientations alternate. Draw a white node at each counterclockwise oriented face and a black node at each clockwise oriented face, and connect nodes whose faces share a corner.

3. Consistency of dimer field theories

3.1 Criteria for consistency and inconsistency

One difficulty in dealing with dimer models is that not all of them produce valid field theories. While there are a number of ways of determining that a dimer produces an invalid field theory there has not yet been a simple criterion for showing that a dimer theory is valid.

One way of proving that a dimer produces an invalid field theory is by counting the number of faces of the dimer, i. e. the number of gauge groups. If the dimer theory is consistent, then the number of gauge groups should equal the number of 0, 2, and 4-cycles in the Calabi-Yau around which D3, D5, and D7-branes, respectively, can wrap [18]. The Euler characteristic of the Calabi-Yau is the number of even dimensional cycles minus the number of odd dimensional cycles. There are no odd dimensional cycles, so the number of gauge groups should be equal to the Euler characteristic. The Euler characteristic of a toric variety equals twice the area of the toric diagram [19].

We propose that a dimer will produce a valid field theory if the dimer has no nodes of valence one and it has a number of faces equal to twice the area of the lattice polygon whose (p, q) -legs are the winding numbers of the zigzag paths. (Recall that this polygon is the same as the Newton polygon of the determinant of the Kasteleyn matrix for consistent theories.) In this section, we will show that dimers satisfying our two criteria also have the properties that their cubic anomalies agree with the Chern-Simons coefficients of the AdS dual, the R -charges of gauge invariant chiral primary operators are greater than or equal to two-thirds, the windings of the zigzag paths are in one-to-one correspondence with the (p, q) -legs of the toric diagram, and the corner perfect matchings are unique.

It will be convenient to introduce a property that we call “proper ordering”, which will turn out to be equivalent to the property of having the correct number of faces and no valence one nodes. We call a node of the dimer *properly ordered* if the order of the zigzag paths around that node is the same as the circular order of the directions of their windings. (We do not allow two zigzag paths with the same winding to intersect, nor do we allow zigzag paths of winding zero, since these scenarios make the ordering ambiguous.) We call a dimer properly ordered if each of its nodes is properly ordered.

Theorem 3.1. *A connected dimer is properly ordered iff it has no valence one nodes and it has a number of faces equal to twice the area of the convex polygon whose (p, q) -legs are*

the winding numbers of the zigzag paths of the dimer.

Proof. A properly ordered dimer cannot have a valence one node, since such a node would be the endpoint of an edge that is an intersection of a zigzag path with itself. Therefore it suffices to prove that a dimer with no valence one nodes is properly ordered iff it has a number of faces equal to twice the area of the convex polygon whose (p, q) -legs are the winding numbers of the zigzag paths of the dimer.

Define the “winding excess” of a node v of the dimer as follows. Let $\mathbf{w}_0, \mathbf{w}_1, \dots, \mathbf{w}_{n-1}$ be the winding numbers of the zigzag paths passing through v (in the order that the paths appear around v). Start at \mathbf{w}_0 and turn counterclockwise to \mathbf{w}_1 , then counterclockwise to \mathbf{w}_2 , etc., and finally counterclockwise back to \mathbf{w}_0 . Then the winding excess is defined as the number of revolutions that we have made minus one. (In the special case where \mathbf{w}_i and \mathbf{w}_{i+1} are equal or one of them is zero, we count one-half of a revolution.) A node is properly ordered iff it has winding excess zero and none of the \mathbf{w}_i are zero and no two consecutive windings are equal. A node with a $\mathbf{w}_i = 0$ or $\mathbf{w}_i = \mathbf{w}_{i+1}$ can have winding excess zero only if it has exactly two edges (and hence two zigzag paths passing through it). There must be some other node that is an endpoint of one of the edges where the two zigzag paths intersect, and that has more than two edges (since the graph is connected). This node cannot have winding excess zero. So all nodes are properly ordered iff all nodes have winding excess zero. A node has negative winding excess iff it has just one edge, and we have assumed that the dimer has no such nodes. Therefore the dimer is properly ordered iff the sum of all of the winding excesses is zero.

If we choose a node and draw all of the wedges between the consecutive winding numbers, then the winding excess is the number of wedges containing any given ray minus one. (We can think of the special case of consecutive winding numbers being the same as the average of a full wedge and an empty wedge, and the case of a zero winding number as the average of wedges of all angles.) Now consider the sum of the winding excess over all vertices. A pair of oppositely oriented intersections between two zigzag paths forms two full wedges and therefore contributes two to the sum. The sum of the contributions from unpaired intersections can be computed as follows. Label the winding numbers $\mathbf{w}_0, \mathbf{w}_1, \dots, \mathbf{w}_{n-1}$, ordered by counterclockwise angle from some ray \mathcal{R} . (A zigzag path with zero winding number has no unpaired intersections, so it is not included.) Then for $i < j$ the unpaired wedges formed by \mathbf{w}_i and \mathbf{w}_j will contain \mathcal{R} iff $\mathbf{w}_i \wedge \mathbf{w}_j < 0$. There are $2|\mathbf{w}_i \wedge \mathbf{w}_j|$ unpaired wedges ($|\mathbf{w}_i \wedge \mathbf{w}_j|$ unpaired crossings of the zigzag paths, and each appears in two vertices). So the number of unpaired wedges formed by \mathbf{w}_i and \mathbf{w}_j containing \mathcal{R} equals $\max(-2\mathbf{w}_i \wedge \mathbf{w}_j, 0) = |\mathbf{w}_i \wedge \mathbf{w}_j| - \mathbf{w}_i \wedge \mathbf{w}_j$. Since $\sum_{i < j} |\mathbf{w}_i \wedge \mathbf{w}_j|$ is the number of unpaired edges, it follows that the number of wedges containing \mathcal{R} is the number of paired edges plus the number of unpaired edges minus $\sum_{i < j} \mathbf{w}_i \wedge \mathbf{w}_j$, or $E - \sum_{i < j} \mathbf{w}_i \wedge \mathbf{w}_j$, where E is the total number of edges of the dimer. The sum of the winding excesses is $E - V - \sum_{i < j} \mathbf{w}_i \wedge \mathbf{w}_j = F - \sum_{i < j} \mathbf{w}_i \wedge \mathbf{w}_j$, where V and F are the number of nodes and faces of the dimer, respectively. We have $\sum_{i < j} \mathbf{w}_i \wedge \mathbf{w}_j = \sum_i \mathbf{w}_i \wedge \sum_{j > i} \mathbf{w}_j$. If we lay the winding vectors tip-to-tail, then $\mathbf{w}_i \wedge \sum_{j > i} \mathbf{w}_j$ is twice the area of the triangle formed by the tail of \mathbf{w}_0 and the tip and tail of \mathbf{w}_i . Hence $\sum_i \mathbf{w}_i \wedge \sum_{j > i} \mathbf{w}_j$ is twice the area of the

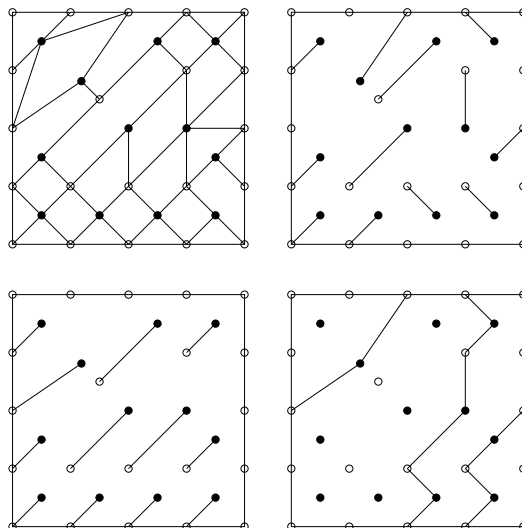


Figure 1: A dimer, two of its corner perfect matchings, and their difference, which is a zigzag path.

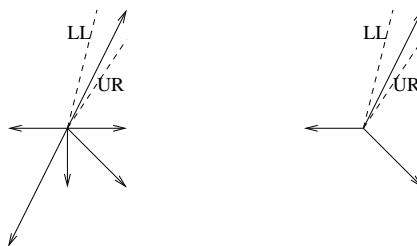


Figure 2: Left: The windings of the zigzag paths of the dimer in figure 1. The dotted lines labeled UR and LL are rays that yield perfect matchings shown in the upper right and lower left quadrants of figure 1, respectively. Right: The windings of the paths passing through the bottom right black node. For any node and any edge ending at that node, the proper ordering criterion implies that the two zigzag paths to which the edge belongs have adjacent winding directions. Therefore in the right diagram, there is a natural correspondence between edges passing through the node and wedges formed by consecutive arrows. When constructing a perfect matching $M(\mathcal{R})$, we choose the wedge containing \mathcal{R} . In the left diagram, there is a one-to-one correspondence between wedges and corners of the toric diagram.

convex polygon formed by all the winding vectors. If we rotate the polygon 90 degrees then we get a polygon whose (p, q) -legs are the winding numbers. So the sum of the winding deficiencies of the nodes is zero iff F equals twice the area of the lattice polygon whose (p, q) -legs are the zigzag path winding numbers. \square

3.2 Some perfect matchings of properly ordered dimers

We will construct some perfect matchings that will turn out to correspond to the corners of the toric diagram. Our construction of the perfect matchings is similar to Theorem 7.2 of [10]. Let \mathcal{R} be any ray whose direction does not coincide with that of the winding number of any zigzag path. For any node v , consider the zigzag paths passing through v whose

winding numbers make the smallest clockwise and smallest counterclockwise angles with \mathcal{R} . (These paths are unique because the proper ordering condition requires that all paths through v have different winding numbers.) By proper ordering, these two zigzag paths must be consecutive around v . Therefore they share an edge that has v as an endpoint. Call this edge $e(v)$. Let v' be the other endpoint of $e(v)$. The same two zigzag paths must be consecutive about v' since they form the edge e . Since v' is properly ordered it must then be the case that those two paths make the smallest clockwise and counterclockwise angles with \mathcal{R} among all paths passing through v' . Hence $e(v) = e(v')$. So the pairing of v with v' is a perfect matching. We will call this matching $M(\mathcal{R})$. Figure 2 depicts the relationship between rays and perfect matchings.

The following characterization of the boundary perfect matchings containing a given edge follows immediately from our definition and will be useful later.

Lemma 3.2. *For any edge e of the dimer, let Z_r and Z_s be the zigzag paths such that e is a positively oriented intersection of Z_r with Z_s . (Equivalently, e is a negatively oriented intersection of Z_s with Z_r .) Let \mathbf{w}_r and \mathbf{w}_s be the windings of Z_r and Z_s , respectively. Let \mathcal{R} be a ray. Then e is in $M(\mathcal{R})$ iff \mathcal{R} is in the wedge that goes counterclockwise from \mathbf{w}_r to \mathbf{w}_s .*

In particular each edge is in at least one corner perfect matching.

3.3 Zigzag paths and (p, q) -legs

As we mentioned in section 2, it is known [8, 9] that dimers that produce a consistent field theory have the property that the (p, q) -legs of the toric diagram are in one-to-one correspondence with the winding numbers of the zigzag paths.

Theorem 3.3. *In a dimer with properly ordered nodes, the zigzag paths are in one-to-one correspondence with the (p, q) -legs of the toric diagram.*

Our proof of Theorem 3.3 resembles that of Theorem 9.3 of [10].

Lemma 3.4. *For any zigzag path Z in any dimer, the number of intersections of a perfect matching with Z is a degree one polynomial function of its coordinates.*

Proof. In computing the Kasteleyn matrix we can choose the path γ_z to follow Z , so that the number of times γ_z intersects a perfect matching M is just the number of edges that M and Z have in common. (See figure 3.) For this choice of γ_z , the point corresponding to M has y -coordinate equal to $|M \cap Z|$. For a different choice of γ_z , the coordinates differ by an affine transformation. \square

Lemma 3.5. *Let Z be a zigzag path of a properly ordered dimer, and let \mathcal{R}_1 and \mathcal{R}_2 be rays such that the winding direction of Z lies between them and all of the other winding directions do not. Then there exists a boundary line of the toric diagram passing through $M(\mathcal{R}_1)$ and $M(\mathcal{R}_2)$ such that all perfect matchings on this line intersect Z exactly $\frac{|Z|}{2}$ times, and all perfect matchings not on the line intersect Z fewer than $\frac{|Z|}{2}$ times.*

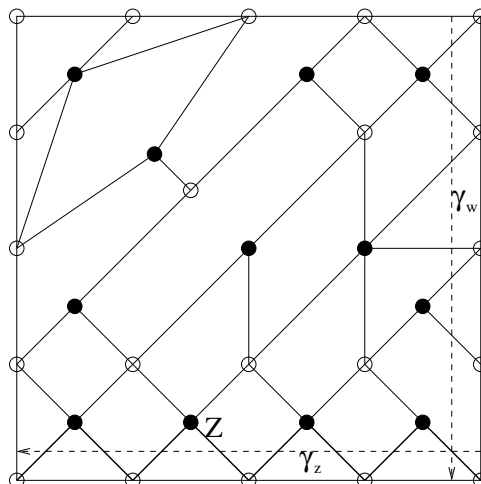


Figure 3: The path γ_z intersects each edge of the zigzag path Z and no other edges. We may choose any path γ_w that completes the basis.

Proof. Since the winding number of Z is adjacent to \mathcal{R}_1 , $M(\mathcal{R}_1)$ must choose one of the two Z -edges of each node that has them. Hence $|M(\mathcal{R}_1) \cap Z| = \frac{|Z|}{2}$ and similarly $|M(\mathcal{R}_2) \cap Z| = \frac{|Z|}{2}$. No perfect matching can contain more than half of the edges of the path. Therefore the toric diagram lies in the half plane that, in the coordinate system of Lemma 3.4, is given by the equation $y \leq \frac{|Z|}{2}$. $M(\mathcal{R}_1)$ and $M(\mathcal{R}_2)$ are both on the boundary. \square

Proposition 3.6. *The matchings $M(\mathcal{R})$ lie on the corners of the toric diagram. The order of the corners around the boundary is the same as the order of the ray directions.*

Proof. The intersection of all half planes described in the proof of Lemma 3.5 is the convex hull of all of the $M(\mathcal{R})$'s. Conversely, each $M(\mathcal{R})$ is in the toric diagram. So the toric diagram must be the convex hull of the $M(\mathcal{R})$'s.

Each $M(\mathcal{R})$ must be at a corner of the toric diagram since it is contained in two different boundary lines (one for the first counterclockwise zigzag path direction from \mathcal{R} and another for the first clockwise zigzag path direction). Furthermore, if \mathcal{R}_1 and \mathcal{R}_2 have only one winding direction between them, then they share a boundary line and hence $M(\mathcal{R}_1)$ and $M(\mathcal{R}_2)$ lie on consecutive corners. \square

Proof of Theorem 3.3. Let \mathbf{w} be the winding number of a zigzag path, and let n be the number of zigzag paths with that winding. Let \mathcal{R}_1 and \mathcal{R}_2 be rays such that \mathbf{w} lies between them and all other winding directions do not. By Proposition 3.6, $M(\mathcal{R}_1)$ and $M(\mathcal{R}_2)$ lie on consecutive corners of the toric diagram. An edge belonging to one of the zigzag paths of winding \mathbf{w} will be in either $M(\mathcal{R}_1)$ or $M(\mathcal{R}_2)$ but not both, while all other edges are in neither or both perfect matchings. Therefore the difference of the two perfect matchings is just the union of the zigzag paths with winding \mathbf{w} . Therefore the toric diagram points corresponding to $M(\mathcal{R}_1)$ and $M(\mathcal{R}_2)$ are separated by $-n\mathbf{w}^\perp$, where $-\mathbf{w}^\perp$ is the 90 degree clockwise rotation of \mathbf{w} . This proves the theorem. \square

3.4 Unique corner perfect matchings

It is generally believed that dimers that have more than one perfect matching at a corner of the toric diagram are inconsistent [5, 20, 8]. We show that properly ordered dimers have unique corner perfect matchings.

Theorem 3.7. *If a dimer is properly ordered, then each corner of the toric diagram has just one perfect matching.*

Proof. Suppose there exists a perfect matching M' that shares a toric diagram point with $M(\mathcal{R})$ but is not equal to $M(\mathcal{R})$. Consider the set of zigzag paths that contain an edge that is in $M(\mathcal{R})$ or M' but not both. Let Z be one with minimal counterclockwise angle from \mathcal{R} . Let v be a node of the dimer through which Z passes. If v includes a zigzag path with winding between \mathcal{R} and that of Z , then $M(\mathcal{R})$ and M' are the same at that vertex. If not, then $M(\mathcal{R})$ chooses one of the edges of Z at v . Recall that Lemma 3.4 says that the number of intersections with Z depends only on the toric diagram point. Therefore M' has the same number of edges in Z as $M(\mathcal{R})$. Since $M(\mathcal{R})$ chooses an edge of Z at every node where $M(\mathcal{R})$ and M' differ, equality can hold only if M' chooses the other edge of Z at every such node. If we start at an edge of Z that is in $M(\mathcal{R})$ but not M' and alternately follow edges of $M(\mathcal{R})$ and M' , then we will traverse a cycle that lies entirely in Z . Since zigzag paths in properly ordered dimers do not intersect themselves, the cycle must be Z . Then both $M(\mathcal{R})$ and M' contain half the edges of Z . So the winding number of Z is either the closest or farthest from \mathcal{R} in the counterclockwise direction. If Z were the farthest, then $M(\mathcal{R})$ and M' would have to be the same because every edge of the dimer would be in at least one zigzag path whose winding is closer to \mathcal{R} in the counterclockwise direction than Z 's. So Z must be the closest in the counterclockwise direction.

Now let Z' be a zigzag path with minimal clockwise angle from \mathcal{R} on which $M(\mathcal{R})$ and M' differ. By the same reasoning as above, we find the winding direction of Z' is the closest to \mathcal{R} in the clockwise direction and that $M(\mathcal{R})$ and M' have no edges of Z' in common. Since Z and Z' represent consecutive sides of the toric diagram, the crossing number of Z and Z' must be nonzero. A node can have two edges belonging to both Z and Z' only if they have opposite orientations, i. e. they contribute zero to the signed crossing number. Therefore there must be a node with only one Z - Z' intersection. M' must include this edge because it includes an edge of Z and Z' at every node that has one, but it cannot include this edge because it does not share any edges of Z with $M(\mathcal{R})$. Therefore our assumption that there existed a matching M' differing from $M(\mathcal{R})$ but sharing the same toric diagram point must be false. \square

Once we know that the corner matchings are unique, we can also classify all of the boundary perfect matchings.

Corollary 3.8. *Consider a point A on the boundary of the toric diagram such that the nearest corner B in the counterclockwise direction is p segments away and the nearest corner C in the clockwise direction is q segments away. Then each perfect matching at A may be obtained from the perfect matching associated to B by flipping p zigzag paths and*

from the perfect matching associated to C by flipping q zigzag paths. The number of perfect matchings at A is $\binom{p+q}{q}$.

Proof. For any boundary perfect matching M there exists a winding \mathbf{w} such that M contains half the edges of each zigzag path of winding \mathbf{w} . For any zigzag path Z of winding \mathbf{w} , we can delete the half of the Z -edges that are in M and add the other half. This operation moves the perfect matching one segment along the boundary of the toric diagram. There can be at most p zigzag paths for which the operation moves the toric diagram point counterclockwise and at most q zigzag paths for which the operation moves the point clockwise. But there are a total of $p + q$ zigzag paths of winding \mathbf{w} , so there must be exactly p of the former and q of the latter. Consequently we see that M can be obtained from a corner perfect matching by flipping p zigzag paths (or from a different corner perfect matching by flipping q zigzag paths). The number of ways of choosing the paths to flip is $\binom{p+q}{p}$. \square

3.5 R -charges and cubic anomalies

The R -charges of the fields may be determined by *a-maximization* [21]. First, we impose the constraint that the R -charge of each superpotential term should be two. We also impose the constraint that the beta function of each gauge group should be zero. These conditions can be expressed as

$$\sum_{e \in v} R(e) = 2 \quad (3.1)$$

$$\sum_{e \in f} [1 - R(e)] = 2. \quad (3.2)$$

Among all $U(1)$ symmetries satisfying these constraints, the R -symmetry is the one that locally maximizes the cubic 't Hooft anomaly

$$a = \frac{9N^2}{32} \left[F + \sum_e (R(e) - 1)^3 \right]. \quad (3.3)$$

Butti and Zaffaroni [20] have proposed some techniques for simplifying the computation of the R -charge. For any perfect matching M we can define a function δ_M that takes the value 2 on all edges in the perfect matching and zero on all other edges. Any such δ_M automatically satisfies (3.1). Butti and Zaffaroni noted that in some cases the perfect matchings on the boundary of the toric diagram yield functions that also satisfy (3.2), and these functions span the set of solutions to (3.1) and (3.2). We will show that their observation is true for properly ordered dimers.

Theorem 3.9. *In a dimer with properly oriented nodes, the solutions to (3.1) and (3.2) are precisely the linear combinations of δ_M , for boundary perfect matchings M .*

We first determine the dimension of the solution space of (3.1) and (3.2), so that we will be able to show that there are not any more solutions beyond the boundary δ_M .

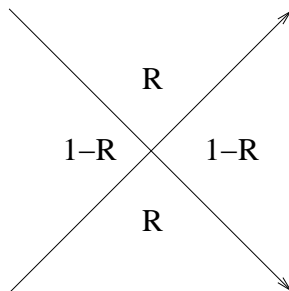


Figure 4: The contribution of the vertex to the equations (3.4) for the four surrounding faces.

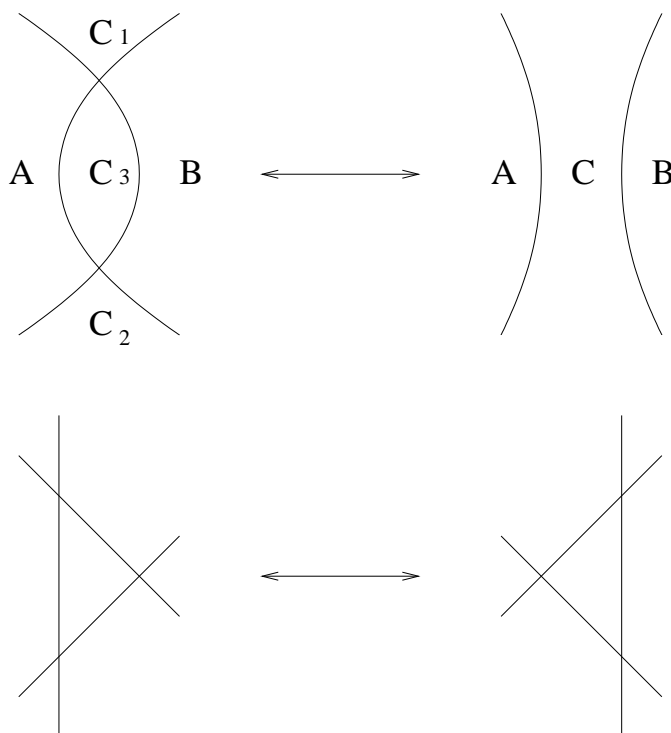


Figure 5: Combinatorial changes in the zigzag path diagram as a result of deformations.

Lemma 3.10. *For any dimer in which the zigzag paths have winding numbers that are prime (i. e. their x and y components are relatively prime, or equivalently, they can each be sent to $(1, 0)$ by an $SL_2(\mathbb{Z})$ transformation) and not all parallel and in which no zigzag path intersects itself, the set of solutions to (3.1) and (3.2) has dimension equal to the number of zigzag paths minus one.*

Proof. First we will show that the number of solutions depends only on the winding numbers of the zigzag paths. We will work with the zigzag path diagram. In this diagram, R is a function on vertices. We can unify (3.1) and (3.2) into a single equation as follows. We first define the function $\sigma_{v,f}(x)$, where v is a vertex of the zigzag path diagram and f is a face of the zigzag path diagram having v as a corner. If the two zigzag paths containing v are similarly oriented around f , then $\sigma_{v,f}(x) = x$; if they are oppositely oriented around f

then $\sigma_{v,f}(x) = 1 - x$. Then (3.1) and (3.2) can be expressed as

$$\sum_{v \in f} \sigma_{v,f}(R(v)) = 2. \quad (3.4)$$

(See figure 4).

We can deform any zigzag path diagram with non-self-intersecting zigzag paths to any other zigzag path diagram with non-self-intersecting zigzag paths with the same winding numbers. As the diagram is deformed, it can change combinatorially in several ways: a pair of intersections between a pair of zigzag paths can be added or removed, or a zigzag path can be moved past the crossing of two other zigzag paths. Figure 5 illustrates these possibilities. Note that at intermediate steps, the zigzag path diagram may not correspond to a dimer, but we can still consider the set of solutions to (3.4).

First consider the case where a pair of intersections between a pair of zigzag paths is added or removed. If C_1 is not the same face as C_2 , then the values of the two new crossings are constrained by the equations for C_1 and C_2 and the dimension of the set of solutions to (3.1) and (3.2) remains unchanged. If the two zigzag paths have winding numbers that are not parallel, then they must intersect somewhere else, which implies $C_1 \neq C_2$. If the winding numbers are parallel, then there must be some other zigzag path whose winding number is not parallel to either and hence must intersect both. Again $C_1 \neq C_2$.

Now consider the case where a zigzag path is moved past the crossing of two other zigzag paths. We can check that any solution to (3.4) in the first diagram is also a solution to (3.4) in the second diagram, and vice versa. So performing the move depicted in the second diagram does not change the solution set. So we have shown that the dimension of the solution space to (3.4) depends only on the winding numbers of the zigzag paths.

In Lemma 6.2 we will exhibit for any set of winding numbers a dimer for which the number of independent solutions to (3.1) and (3.2) is the number of zigzag paths minus one. \square

Lemma 3.10 tells us how to solve (3.1) and (3.2) for a large class of dimers, many of which are not properly ordered. It is interesting to note that the second move shown in figure 5 does not change either a or $\sum_e (1 - R(e))$. The first move also leaves a and $\sum_e (1 - R(e))$ invariant in the case where the two zigzag paths are oppositely oriented (the charges of the introduced vertices sum to two and $(R_1 - 1)^3 + (R_2 - 1)^3 = (R_1 + R_2 - 2) [(R_1 - 1)^2 - (R_1 - 1)(R_2 - 1) + (R_2 - 1)^2]$). When the zigzag path diagram corresponds to a dimer, $\sum_e (1 - R(e))$ is the number of faces in the dimer.

Proof of Theorem 3.9. First we will show that the δ_M are solutions to (3.2). Suppose a face f with $2n$ sides had n of those sides in a boundary perfect matching M . (A side of a face is an edge of the face along with a normal pointing into the face. If a face borders itself then the bordering edge is part of two different sides of the face. If a self-border edge is in a perfect matching, then we count two sides of f in that perfect matching.) From Corollary 3.8, we know that we can get from M to any other boundary perfect matching by flipping zigzag paths. Note that this operation leaves invariant the number of sides of

each face in the perfect matching. Therefore every boundary perfect matching has n sides of f . So every node of f selects one of the two adjacent sides of f for all boundary perfect matchings. By Lemma 3.2 we know that every edge is in some corner perfect matching. So the only edges belonging to any node of f are the adjacent sides of f . Therefore, as we move along the boundary of the face we are following a zigzag path. But then we have a zigzag path with zero winding, which violates proper ordering. So the assumption that a face with $2n$ sides can have n sides in a boundary perfect matching must be false. Therefore a face with $2n$ sides can have at most $n - 1$ sides in a boundary perfect matching. Sum this inequality over all faces:

$$\sum_f \sum_{s \in f \cap M} 1 \leq \sum_f \left[\left(\sum_{s \in f} \frac{1}{2} \right) - 1 \right] \quad (3.5)$$

where f runs over faces and s runs over sides. Now reverse the order of the sums:

$$\sum_{s \in M} \sum_{f \ni s} 1 \leq \sum_s \sum_{f \ni s} \frac{1}{2} - F \quad (3.6)$$

$$V \leq (2E) \left(\frac{1}{2} \right) - F \quad (3.7)$$

$$V \leq E - F. \quad (3.8)$$

Since we know $V = E - F$, equality must have held in each case. So (3.2) is satisfied by boundary perfect matchings.

The difference between any two boundary perfect matchings is a sum of functions δ_Z , where Z is a zigzag path and the value δ_Z alternates between 2 and -2 on Z and is zero outside of Z . The only relation obeyed by the δ_Z is that they sum to zero. So the dimension of the space of solutions to (3.1) and (3.2) that we have found equals the number of zigzag paths minus one. By Lemma 3.10, there can be no more solutions. \square

When some of the boundary points of the toric diagram are not corners, there are many sets of perfect matchings that form a basis for the solutions to (3.1) and (3.2). We will construct a basis by associating each segment of the boundary of the toric diagram with a zigzag path, and choosing one perfect matching at each boundary point so that the difference between two consecutive perfect matchings is the zigzag path corresponding to the segment between them. Write $R = \sum_i \lambda_i \delta_{M_i}$, where M_i are the perfect matchings in the basis and the λ_i are real numbers.

Butti and Zaffaroni [20] also noted that in many cases each edge that is a positively oriented intersection of a zigzag path Z_r with another zigzag path Z_s occurs in the perfect matchings in $cc(r, s)$, the counterclockwise segment from r to s , while a negatively oriented intersection of Z_r with Z_s occurs in the perfect matchings not in $cc(r, s)$. In this case, the value of $R - 1$ for a positively oriented intersection of Z_r with Z_s is $2 \left(\sum_{i \in cc(r, s)} \lambda_i \right) - 1$. For a negatively oriented intersection the value of $R - 1$ is $2 \left(\sum_{i \notin cc(r, s)} \lambda_i \right) - 1$, which equals $- \left[2 \left(\sum_{i \in cc(r, s)} \lambda_i \right) - 1 \right]$ since $\sum_i \lambda_i = 1$. So then the total contribution to $\sum_e (R - 1)^3$

from the intersections of Z_r with Z_s is $(\mathbf{w}_r \wedge \mathbf{w}_s) \left[2 \left(\sum_{i \in cc(r,s)} \lambda_i \right) - 1 \right]^3$. Hence (3.3) can be rewritten as

$$a = \frac{9N^2}{32} \left[F + \sum_{r < s} (\mathbf{w}_r \wedge \mathbf{w}_s) \left(2 \left(\sum_{i \in cc(r,s)} \lambda_i \right) - 1 \right)^3 \right]. \quad (3.9)$$

Proposition 3.11. *If a dimer has properly oriented nodes, then it is the case that all positively (resp. negatively) oriented intersections of Z_r with Z_s are in precisely the perfect matchings that are in $cc(r, s)$ (resp. $cc(s, r)$). Hence 3.9 holds for properly ordered dimers.*

Proof. Assume that the dimer has properly ordered nodes. As we go around the toric diagram, the perfect matching switches from containing an edge e to not containing it only if we changed the perfect matching by a zigzag path containing e . So each intersection of Z_r with Z_s occurs in either the perfect matchings in $cc(r, s)$ or the perfect matchings in its complement. From Lemma 3.2 we know that the positively oriented intersections are in the corners of $cc(r, s)$ and the negatively oriented intersections are not. \square

A particularly nice rearrangement of (3.9) that we will find useful is [15, 22]

$$a = \frac{9N^2}{4} \sum_{ijk} \text{area}(P_i P_j P_k) \lambda_i \lambda_j \lambda_k. \quad (3.10)$$

where P_i is the point on the toric diagram corresponding to the i th perfect matching. This formula tells us that the triangle anomaly of the three symmetries with respective charges δ_{M_i} , δ_{M_j} , and δ_{M_k} is $N^2 \text{area}(P_i P_j P_k)$. AdS-CFT predicts that the U(1) symmetries of the CFT correspond to gauge symmetries in the AdS theory, and that the triangle anomalies of the CFT should equal the corresponding Chern-Simons coefficients in the AdS theory [3]. The Chern-Simons coefficients are indeed found to be $N^2 \text{area}(P_i P_j P_k)$ [15]. So the field theory produced by a properly ordered dimer will have precisely the cubic anomalies predicted by the AdS theory. This is strong evidence that properly ordered dimers are consistent.

3.6 Unitarity bound

Gauge invariant scalar operators in a four-dimensional CFT must have dimension at least one [16]. We also have the BPS bound $\Delta \geq \frac{3}{2}|R|$, where Δ is the dimension of an operator and R is its R -charge. Equality is achieved in the case of chiral primary operators [17]. So in order for the theory to be physically valid it is necessary that the gauge invariant chiral primary operators have R -charge at least $\frac{2}{3}$.

Theorem 3.12. *If a can be expressed in the form (3.10), then there exists an N such that in the dimer theory with N colors, each gauge invariant chiral primary operator has R -charge at least $\frac{2}{3}$. In particular properly ordered dimers have this property.*

Lemma 3.13. *At the point where a is locally maximized, the weight of each corner perfect matching is positive, and the weight of the other boundary perfect matchings is zero.*

Proof. This follows immediately from equation (4.2) of [20]. \square

Lemma 3.14 (A. Kato [23]). *If a is given by (3.10), then at the point where a is locally maximized,*

$$\frac{\partial a}{\partial \lambda_i} = 3a. \quad (3.11)$$

Proof. We can use Lagrange multipliers to find the local maximum of a .

$$\frac{\partial a}{\partial \lambda_i} = \mu \frac{\partial}{\partial \lambda_i} \sum_j \lambda_j = \mu \quad (3.12)$$

for some constant μ . Since a is homogeneous of degree three,

$$3a = \sum_i \lambda_i \frac{\partial a}{\partial \lambda_i} \quad (3.13)$$

$$= \sum_i \lambda_i \mu \quad (3.14)$$

$$= \mu. \quad (3.15)$$

□

Lemma 3.15 (A. Kato [23]). *At the point where a is locally maximized, each λ_i is at most $\frac{1}{3}$.*

Proof. By Lemma 3.14, $3\lambda_i a = \lambda_i \frac{\partial a}{\partial \lambda_i}$. Since every term of a is degree zero or one in λ_i , the right-hand side is simply the terms of a containing λ_i . We can see from (3.10) that the coefficient of each term of a is nonnegative and from Lemma 3.13 that each λ_i is nonnegative when a is maximized. Hence the sum of the terms of a containing λ_i is at most a . Therefore $3\lambda_i a \leq a$, so $\lambda_i \leq \frac{1}{3}$. □

Proof of Theorem 3.12. First consider the mesonic operators, which arise as the trace of a product of operators corresponding to the edges around a loop of the quiver. The number of signed crossings between a loop and a perfect matching of the dimer is an affine function of the perfect matching's position in the toric diagram. If the loop has nonzero winding, then the function is not constant, and its zero locus is a line. This line can intersect the corners of the toric diagram at most twice. Therefore each loop intersects all but at most two of the corner perfect matchings. The sums of the weights of those two perfect matchings is at most $\frac{2}{3}$, and from Lemma 3.13 we know that the non-corner matchings have weight zero. The sum of the weights of the perfect matchings that do intersect the loop is then at least $\frac{1}{3}$. So the loop has R -charge at least $\frac{2}{3}$. The R -charge of a loop with zero winding is twice the number of intersections it has with any perfect matching. Every edge is in at least one perfect matching so this number must be positive. So a loop with zero winding has R -charge at least 2.

The theory also has baryonic operators. If the gauge groups are $SU(N)$ then these operators are the N th exterior powers the bifundamental fields. Each edge of the dimer is contained in at least one corner perfect matching by Lemma 3.2, and we know from Lemma 3.13 that each corner of the toric diagram has a positive contribution to the R -charge. So each dimer edge has positive R -charge. For sufficiently large N , the corresponding baryonic operator will have R -charge at least $\frac{2}{3}$. □

4. Bounds on a

4.1 Bounds on a for toric theories

We can use (3.10) to establish bounds for a . In this section we let the indices ijk of the perfect matchings run over the corner perfect matchings only, since we know from Lemma 3.13 that the non-corner perfect matchings have weight zero.

Theorem 4.1. *Let N be the number of colors of each gauge group, and let K be the area of the toric diagram (which is half the number of gauge groups). Then*

$$\frac{27N^2K}{8\pi^2} < a \leq \frac{N^2K}{2}. \quad (4.1)$$

The upper bound is achieved iff the toric diagram is a triangle, and the lower bound is approached as the toric diagram approaches an ellipse.

Proof of the lower bound of Theorem 4.1. The polar body X_R^* of a convex polygon X with respect to the point R is defined as the set of points Q satisfying $\overrightarrow{RQ} \cdot \overrightarrow{RP} \leq 1$ for all $P \in X$. Recall that maximizing a is equivalent to minimizing the volume of a slice of the dual toric cone [24, 20]. More specifically, if \vec{r} is the three-dimensional Reeb vector, then $\frac{9N^2}{8a}$ is the volume of the set of points \vec{x} in the dual cone satisfying $\vec{r} \cdot \vec{x} \leq 3$. The cross section of the dual cone in the plane $\vec{r} \cdot \vec{x} = 3$ is the polar body of the toric diagram with respect to the Reeb vector (considered as a point in the plane of the toric diagram). If we call the toric diagram X , then $\frac{27N^2}{8a} = \inf_{R \in X} \text{area}(X_R^*)$. Then the statement of the lower bound is equivalent to $\text{area}(X) \inf_{R \in X} \text{area}(X_R^*) < \pi^2$. The result $\text{area}(X) \inf_{R \in X} \text{area}(X_R^*) \leq \pi^2$ was proved by Blaschke [25, 26]; equality occurs in the case of an ellipse. Since the toric diagram is a polygon, it cannot be perfectly elliptical and hence equality does not hold. \square

We will need to use the following results for the proof of the upper bound.

Proposition 4.2 (A. Kato [23]). *The local maximum of a is the overall maximum of a in the region $\lambda_i \geq 0, \sum_i \lambda_i = 1$.*

Proposition 4.3 (A. Butti and A. Zaffaroni [20]). *Let R be a point in the interior of the toric diagram. Define*

$$f_i = \frac{\text{area}(P_{i-1}P_iP_{i+1})}{\text{area}(P_{i-1}P_iR) \text{area}(P_iP_{i+1}R)} \quad (4.2)$$

$$S = \sum_i f_i \quad (4.3)$$

$$\lambda_i = f_i/S. \quad (4.4)$$

Then the following results hold:

$$R = \sum_i \lambda_i P_i \quad (4.5)$$

$$a = \frac{27N^2}{2S}. \quad (4.6)$$

Furthermore, when R is the Reeb vector and the λ_i are given by (4.4), a is locally maximized (over all choices of λ_i , not just those of the form (4.4)).

Proof of the upper bound of Theorem 4.1. We use induction on the number of corners of the toric diagram. If the toric diagram is a triangle, then a is maximized when each λ_i is $\frac{1}{3}$. So $a = \frac{9N^2}{4}K(3!)(\frac{1}{3})^3 = \frac{N^2K}{2}$.

Assume the toric diagram has more than three corners. Let λ_i^M be the values of λ_i for which a is locally maximized. Choose a particular i and let $\lambda_i^D = 0$, $\lambda_{i+1}^D = \lambda_i^M + \lambda_{i+1}^M$, and $\lambda_j^D = \lambda_j^M$ for all other j . We will define $a^M = a|_{\lambda^M}$, $a^D = a|_{\lambda^D}$, and $\Delta a = a^D - a^M$. Since a has degree one in each individual λ_j ,

$$\Delta a = \left. \frac{\partial a}{\partial \lambda_i} \right|_{\lambda^M} (-\lambda_i^M) + \left. \frac{\partial a}{\partial \lambda_{i+1}} \right|_{\lambda^M} \lambda_i^M + \left. \frac{\partial^2 a}{\partial \lambda_i \partial \lambda_{i+1}} \right|_{\lambda^M} (-\lambda_i^M)(\lambda_i^M) \quad (4.7)$$

Recall that since a is initially maximized, $\left. \frac{\partial a}{\partial \lambda_i} \right|_{\lambda^M} = \left. \frac{\partial a}{\partial \lambda_{i+1}} \right|_{\lambda^M}$ and hence the first two terms of (4.7) cancel. Now use (3.10) to expand the last term:

$$\Delta a = -\frac{27N^2}{2}(\lambda_i^M)^2 \sum_j \lambda_j^M \text{area}(P_i P_{i+1} P_j). \quad (4.8)$$

Since all of the P_j are on the same side of the line $P_i P_{i+1}$,

$$\Delta a = -\frac{27N^2}{2}(\lambda_i^M)^2 \text{area}(P_i P_{i+1} R) \quad (4.9)$$

where R is the weighted center of mass of the P_j with weights λ_j^M . Now apply Proposition 4.3. We can write

$$\Delta a = -\lambda_i^M \frac{27N^2 \text{area}(P_{i-1} P_i P_{i+1})}{2S \text{area}(P_{i-1} P_i R)} \quad (4.10)$$

$$= -\lambda_i^M a^M \frac{\text{area}(P_{i-1} P_i P_{i+1})}{\text{area}(P_{i-1} P_i R)}. \quad (4.11)$$

Since $\sum_i \lambda_i^M = 1$ and $\sum_i \text{area}(P_{i-1} P_i R) = K$, there must be some i for which $\frac{\lambda_i^M}{\text{area}(P_{i-1} P_i R)} \leq \frac{1}{K}$. For such an i ,

$$-\frac{\Delta a}{a^M} \leq \frac{\text{area}(P_{i-1} P_i P_{i+1})}{K} \quad (4.12)$$

Note that $\text{area}(P_{i-1} P_i P_{i+1})$ is the amount by which K would decrease if we removed P_i from the toric diagram. Since $\lambda_i^D = 0$, the λ_j^D are a valid choice of weights for the toric diagram with P_i removed. Then

$$-\frac{\Delta a}{a^M} \leq -\frac{\Delta K}{K}. \quad (4.13)$$

Therefore $\frac{a^D}{K + \Delta K} \geq \frac{a^M}{K}$. By Proposition 4.2 the local maximum value of a for the new toric diagram is at least as large as a^D . We want to show that it is strictly larger, or equivalently, that λ_j^D do not locally maximize a for the new toric diagram. Recall from Lemma 3.14 that a is locally maximized when $\frac{\partial a}{\partial \lambda_{i+1}} = 3a$. Hence a will continue to be maximized only if $\Delta \frac{\partial a}{\partial \lambda_{i+1}} = 3\Delta a$. Once again we use the fact that a is degree one in each individual λ_j :

$$\Delta \frac{\partial a}{\partial \lambda_{i+1}} = \left. \frac{\partial^2 a}{\partial \lambda_i \partial \lambda_{i+1}} \right|_{\lambda^M} (-\lambda_i^M) \quad (4.14)$$

$$= \frac{\Delta a}{\lambda_i^M}. \quad (4.15)$$

Equation in [27]	(x,y,z)	$(9-n)(\alpha x^2 + \beta y^2 + \gamma z^2)$
(1)	(1, 1, 1)	27
(1)	(1, 1, 2)	54
(1)	(1, 2, 5)	270
(2)	(1, 1, 1)	32
(3)	(1, 1, 1)	36
(4)	(1, 2, 1)	50
(5)	(1, 1, 1)	32
(6.1)	(1, 1, 1)	27
(6.2)	(2, 1, 1)	36
(7.1)	(2, 2, 1)	32
(7.2)	(2, 1, 1)	32
(7.3)	(3, 1, 1)	36
(8.1)	(3, 3, 1)	27
(8.2)	(4, 2, 1)	32
(8.3)	(3, 2, 1)	36
(8.4)	(5, 2, 1)	50

Table 1: The values of $\frac{54N^2K}{a} = (9-n)(\alpha x^2 + \beta y^2 + \gamma z^2)$ for some of the quiver gauge theories defined in [27]. Note that the equations in [27] have infinitely many solutions (which can be seen by observing that if we fix one of x, y, z we get a form of Pell's equation), so there exist theories with arbitrarily large $\frac{54N^2K}{a}$.

Hence a can continue to be maximized only if $\lambda_i^M = \frac{1}{3}$. But λ_{i+1}^M is positive (since we chose to let our indices enumerate corner perfect matchings only), so $\lambda_{i+1}^D = \lambda_i^M + \lambda_{i+1}^M > \frac{1}{3}$. By Lemma 3.15, λ_j^D cannot be the local maximum point. By the induction hypothesis, the new $\frac{a}{K}$ is at most $\frac{1}{2}$, so the old $\frac{a}{K}$ must be smaller than $\frac{1}{2}$. \square

4.2 Comparison to non-toric field theories

Let us consider how we might formulate a similar bound for non-toric CFTs. We need to decide how to interpret K in the non-toric case. It seems natural to replace $2N^2K$ with the sum of the squares of the numbers of colors of each gauge group.

Let's look at the values of $\frac{a}{N^2K}$ for a cone over a del Pezzo surface. Reference [27] lists some quiver gauge theories that are dual to these Calabi-Yaus. In their notation, the sum of the squares of the number of colors is $\alpha x^2 + \beta y^2 + \gamma z^2$. We can compute a by looking at the AdS dual theory. References [28, 29] tell us that $\frac{\pi^3}{4a}$ is the volume of the horizon, and [30] tells us that the volume of the real cone over dP_n is $\frac{\pi^3(9-n)}{27}$. So $a = \frac{27}{4(9-n)}$. So then $\frac{54N^2K}{a} = (9-n)(\alpha x^2 + \beta y^2 + \gamma z^2)$, and the bound (4.1) for toric theories is then equivalent to $27 \leq (9-n)(\alpha x^2 + \beta y^2 + \gamma z^2) < 4\pi^2$. From table 1 we see that the toric upper bound on $\frac{54N^2K}{a}$ is not true for all quiver gauge theories. In fact, $\frac{N^2K}{a}$ can be arbitrarily large. Equation (1) of [27] is $x^2 + y^2 + z^2 = 3xyz$. If we set $z = 1$ then we have a Pell's equation in x and y and there are infinitely many solutions. On the other hand,

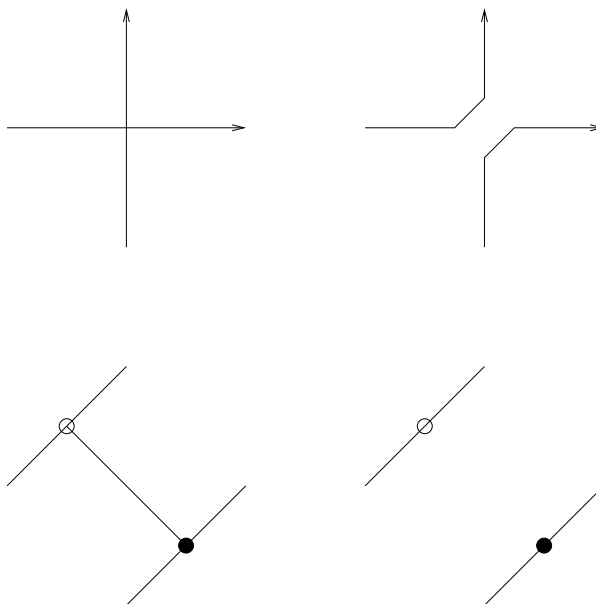


Figure 6: Top: Merging two zigzag paths by deleting the intersection between them. Bottom: The effect on the dimer.

$27 \leq (9 - n)(\alpha x^2 + \beta y^2 + \gamma z^2)$ still holds for all of the theories considered in [27]. It would be interesting to know if the inequality holds more generally.

5. Merging zigzag paths

5.1 Deleting an edge of the dimer

Theorem 3.3 says that, if a dimer is properly ordered, then we can determine its toric diagram from the windings of its zigzag paths. As we mentioned in section 3.3, Hanany and Vegh [8] and Stienstra [10] have previously made proposals for drawing a dimer with given zigzag winding numbers, but their procedures are impractical for large dimers because of the large amount of trial and error required.

Partial resolution [11 – 14] has previously been suggested as a method of determining the dimer from the quiver [13, 31, 5]. It involves starting with a toric diagram whose dimer model is known and introducing Fayet-Iliopoulos terms that Higgs some of the fields and remove part of the toric diagram to create a new diagram. However, as is the case with the Fast Inverse Algorithm, the previous proposals involving partial resolution suffered from being computationally infeasible.

In this section, we will explore how certain operations on the dimer affect its zigzag paths. These operations can be interpreted as partial resolutions. We will later use these operations to construct an algorithm for drawing a properly ordered dimer with given winding numbers that requires no trial and error.

One operation that we can perform is to remove an intersection of two zigzag paths (or equivalently, delete an edge of the dimer). The operation has the effect of merging the two paths into a single path. An example is shown in figure 6. In physical terms, we are

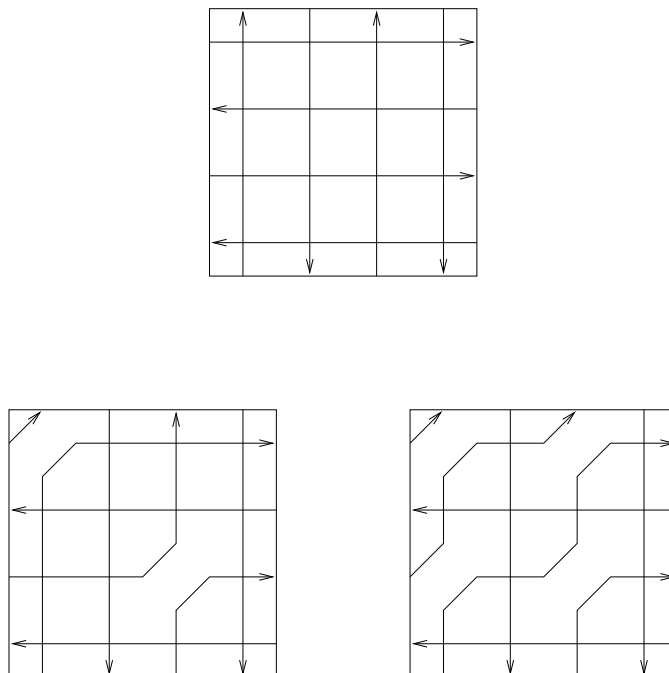


Figure 7: Left: An incorrect way of making two $(1,1)$ paths. They intersect each other, which implies that the adjacent nodes are not properly ordered. Right: The correct way of making two $(1,1)$ paths.

Higgsing away the edge by turning on Fayet-Iliopoulos parameters for the adjacent faces. This is an example of partial resolution of the toric singularity [11–14]. We will always merge paths that intersect just once. In the following we will sometimes assume that the windings of the paths are $(1, 0)$ and $(0, 1)$; any other case is $SL_2(\mathbb{Z})$ equivalent to this one.

5.2 Making multiple deletions

Suppose we want to make $n > 1$ $(1, 1)$ edges from $(1, 0)$ and $(0, 1)$ edges. If we make them one at a time, then we would violate the proper ordering of nodes because we would have $(1, 1)$ paths intersecting each other. We should instead delete all n^2 edges between the n $(1, 0)$ edges and the n $(0, 1)$ edges. We will refer to this procedure as Operation I.

5.3 Extra crossings

We mentioned in section 2 that the number of oriented crossings between a pair of paths is a function only on their windings. The number of unoriented crossings is greater than or equal to the absolute value of the number of oriented crossings. If equality does not hold then we say that the pair of paths has “extra crossings”. We say that a diagram has extra crossings if any pair of its paths does. There is nothing inherently wrong with extra crossings, but we may find it desirable to produce diagrams without them.

The edge deletion procedure mentioned in the previous section sometimes introduces extra crossings. An example of this is shown in figure 8. We combine a $(1, 0)$ zigzag path and a $(0, 1)$ to make a $(1, 1)$ zigzag path, and we also combine $(-1, 0)$ and $(0, -1)$ paths to make

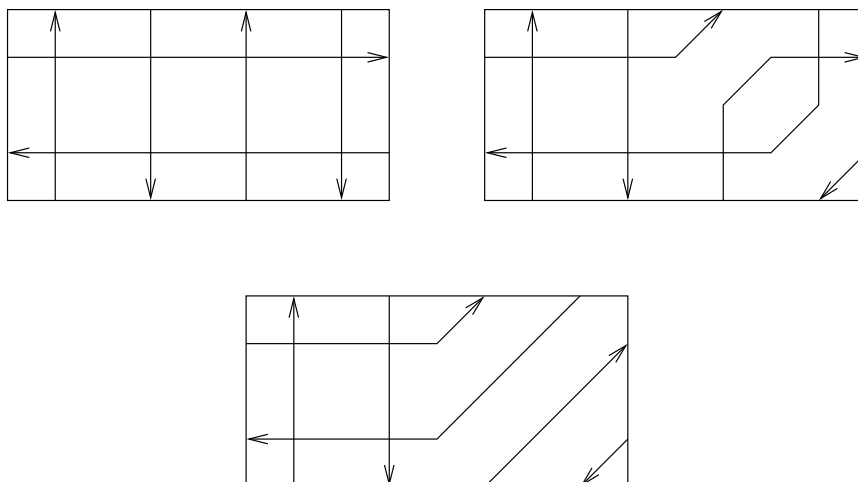


Figure 8: The top left diagram has no extra crossings. The top right diagram shows what happens when some zigzag paths are merged. The two diagonal paths now have extra crossings with each other. The bottom diagram shows what happens when we move the two zigzag paths past each other; they no longer intersect.

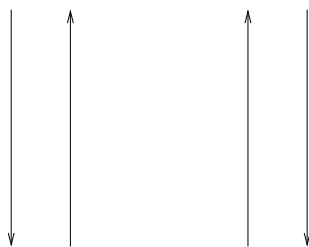


Figure 9: Pairs of paths that are positively and negatively oriented, respectively.

a $(-1, -1)$ path. The $(1, 1)$ path and $(-1, -1)$ path have a positively oriented intersection coming from the $(0, 1) - (-1, 0)$ intersection and a negatively oriented intersection coming from the $(1, 0) - (0, -1)$ intersection. Note that we can get rid of these crossings by moving the two paths past each other. In terms of the dimer, moving the paths past each other merges the two vertices adjacent to a valence two node. Physically, we are integrating out a mass term.

We define a pair of zigzag paths to be an “opposite pair” if they have opposite winding numbers, they do not intersect, and they bound a region containing no crossings. Also, we define the orientation of an opposite pair to be positive if the area containing no crossings is to the left of an observer traveling along one of the paths, and negative if the area is on the right. (See figure 9.) We have just seen how to take a pair negatively oriented horizontal paths and a pair of negatively oriented vertical paths and turn them into a pair of negatively oriented diagonal paths. Similarly we can turn a pair of positively oriented horizontal paths and a pair of positively oriented vertical paths into a pair of positively oriented diagonal paths. In terms of dimers, this operation takes a node of valence four, deletes two opposite edges, and merges the other endpoints of the two remaining edges.

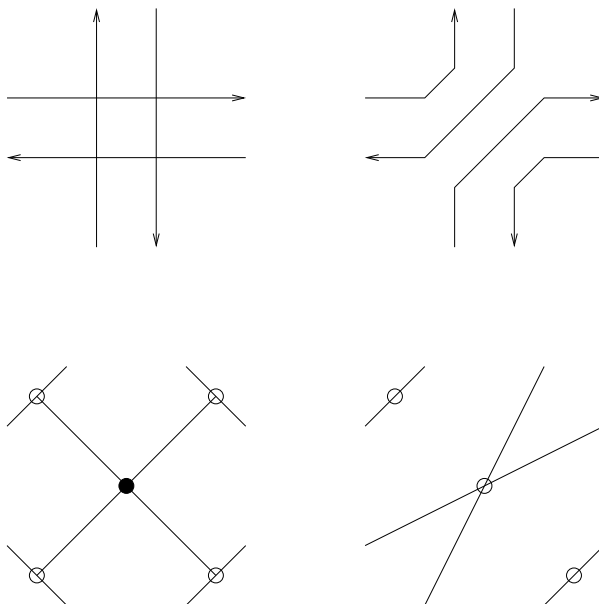


Figure 10: Making $(1,1)$ and $(-1,1)$ paths from horizontal and vertical paths in the zigzag path picture and the dimer picture.

figure 10 shows the operation in terms of both zigzag paths and dimers.

More generally, we can make n $(1,1)$ paths and n $(-1,-1)$ paths and get rid of their crossings. An example is given in figure 11. We have to untangle each $(1,1)$ path from each $(-1,-1)$ path. Note that all $2n$ paths must have the same orientation. We will call this procedure Operation II.

If we want to create differing numbers of $(1,1)$ and $(-1,-1)$ paths, then we run into the problem that we cannot pair them all. We will need to do something more complicated. Let m be the number of $(1,1)$ paths we want to make, and let n be the number of $(-1,-1)$ paths we want to make. Assume $m > n$. We first make $m - n$ $(1,1)$ paths. Now we completely remove n pairs of adjacent $(1,0)$ and $(-1,0)$ paths and n pairs of adjacent $(0,1)$ and $(0,-1)$ paths. Because the pairs are adjacent, the condition that intersection orientations alternate along a path is preserved. Now we want to insert n pairs of adjacent $(1,1)$ and $(-1,1)$ paths, and we want to make sure that there are no extra crossings. This can be accomplished by making them follow one of the $m - n$ already existing $(1,1)$ paths. An example is given in figure 12. Figure 13 shows what removing or adding a pair of zigzag paths does to the dimer. This procedure will be called Operation III.

6. An efficient inverse algorithm

6.1 Description of the algorithm

In describing the algorithm we find it useful to draw toric diagrams rotated 90 degrees counterclockwise from their usual presentation. Our convention will make the algorithm easier to visualize, because it makes the windings of the zigzag paths equal to, rather than perpendicular to, the vectors of the toric diagram edges.

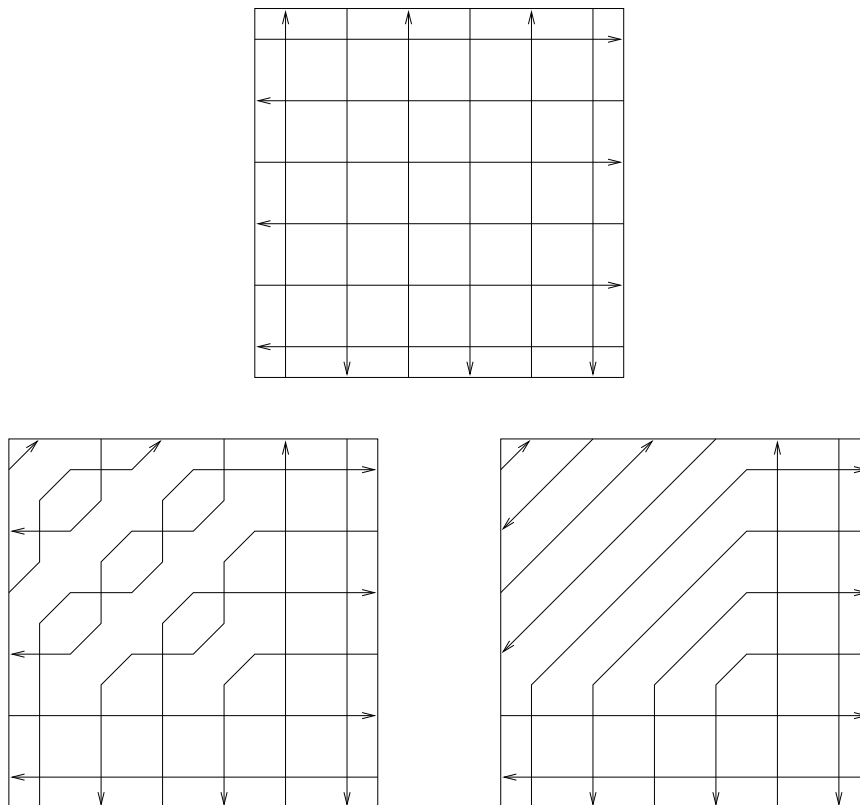


Figure 11: Creating two $(1, 1)$ and two $(-1, -1)$ paths from horizontal and vertical paths. We first merge horizontal and vertical paths to create diagonal paths, then move the diagonal paths past each other.

Let X be a toric diagram for which we would like to construct a dimer. Let Y be the smallest rectangle with horizontal and vertical sides that contains X . Since Y represents an orbifold of the conifold, we know a dimer for Y . We will modify this dimer until we get a dimer for X .

Before we begin, we need to make the following definition. A tangent line to a convex polygon P is a line ℓ such that $\ell \cap P \subseteq \partial P$ and $\ell \cap P \neq \emptyset$. Note that a convex polygon has exactly two tangent lines with a given slope.

We begin by finding the slope one tangent lines to X and cutting Y along these lines to produce some $(1, 1)$ and $(-1, -1)$ paths. We use Operation I if the number of $(1, 1)$ or $(-1, -1)$ paths desired is zero, Operation II if the numbers are equal, and Operation III if the numbers are both nonzero and unequal. Next we want to cut along the slope $1/2$ tangent lines to X to produce $(2, 1)$ and $(-2, -1)$ paths. In fact we already know how to do this, because $SL_2(\mathbb{Z})$ equivalence reduces the problem of making $(2, 1)$ and $(-2, -1)$ paths from $(1, 0)$, $(-1, 0)$, $(1, 1)$, and $(-1, -1)$ paths to the problem of making $(1, 1)$ and $(-1, 1)$ paths from $(1, 0)$, $(-1, 0)$, $(0, 1)$ and $(0, -1)$ paths. Hence we can now cut Y along the slope $1/2$ tangent lines to X . Similarly, we can cut Y along the slope 2 tangent lines to X . After this, we can make $(3, 1)$ paths by combining $(1, 0)$ and $(2, 1)$ paths, $(3, 2)$ paths by combining $(1, 1)$ and $(2, 1)$ paths, etc. We can eventually make paths of all slopes, with

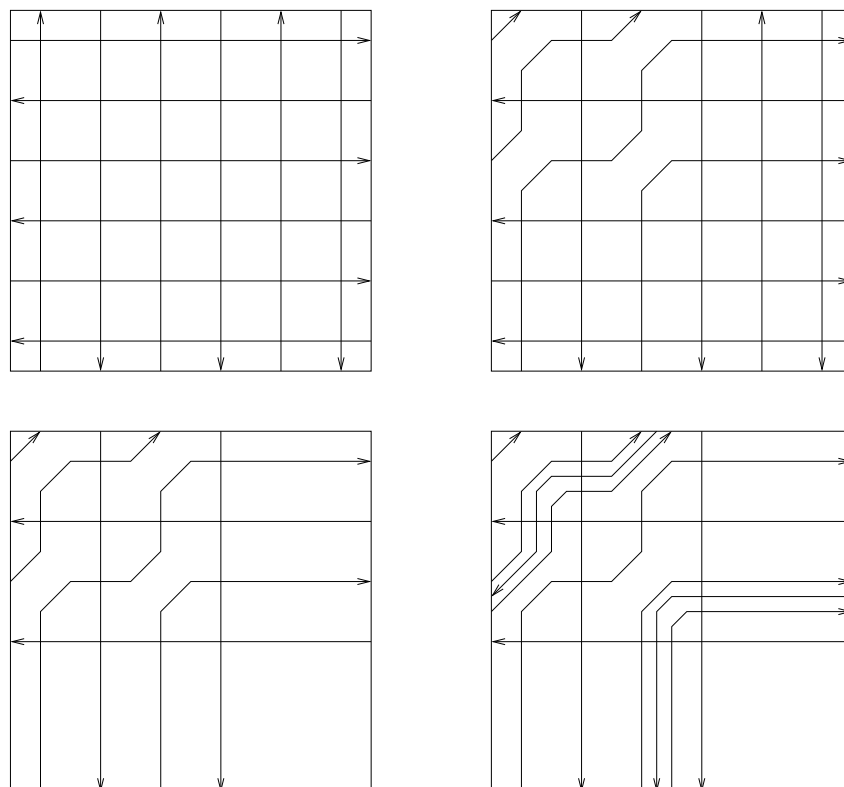


Figure 12: Creating three $(1, 1)$ paths and one $(-1, 1)$ path without introducing extra crossings. We first make two $(1, 1)$ paths and then add a $(1, 1) - (-1, -1)$ pair that follows one of those two paths.

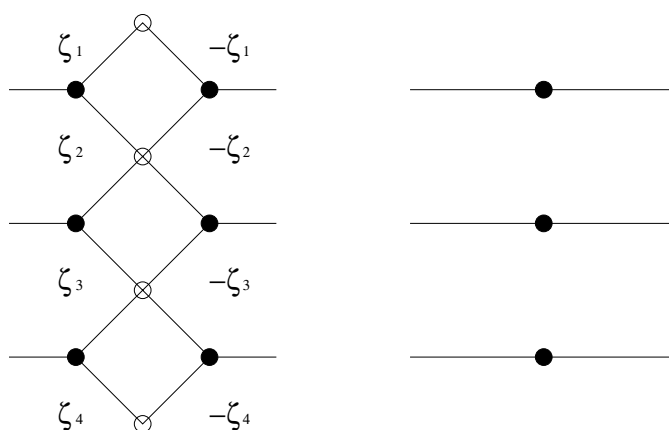


Figure 13: Left: a dimer with a pair of adjacent opposite zigzag paths. Right: the dimer with the paths removed. In physical terms, we are introducing performing a partial resolution by introducing Fayet-Iliopoulos parameters for the faces on either side of the diamonds [11 – 14]. (In particular note that the resolution of the double conifold in [14] is an example of this operation.) For each pair of faces that meet at one of the points in the middle, their FI parameters should sum to zero. All parameters on the left should have the same sign.

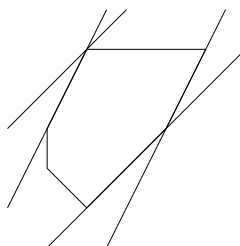


Figure 14: Some tangent lines to a convex polygon.

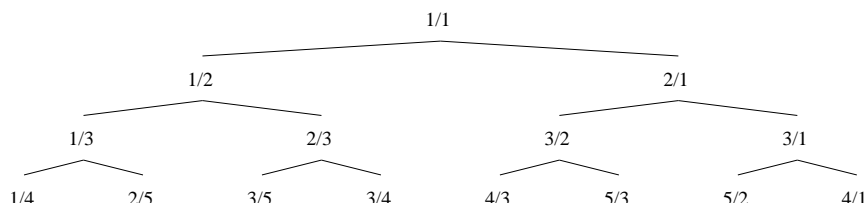


Figure 15: The Farey tree tells us the order in which to make zigzag paths. For example, in order to make $(3, 4)$ zigzag paths we first make $(1, 1)$ zigzag paths, then $(1, 2)$ paths, then $(2, 3)$ paths.

the order in which we make the paths determined by the Farey tree. (See figure 15.) We can then enumerate over all negative slopes, starting with -1 . When we are finished, we will have a dimer for X .

Figure 16 shows an example case of the algorithm.

6.2 Proof of the algorithm

We need to prove that we have the paths necessary to perform each step, and that the finished dimer has properly ordered nodes and has no extra crossings.

Theorem 6.1. *At each step of the algorithm, the following are true:*

1. *If there are m zigzag paths with winding (a, b) and n zigzag paths with winding $(-a, -b)$, then there are $\min(m, n)$ negatively oriented pairs of (a, b) and $(-a, -b)$ paths. (This condition ensures that we can always perform the next step of the algorithm.)*
2. *There are no extra crossings.*
3. *All nodes are properly ordered.*

Proof. It is clear that all of these conditions hold for the initial dimer. Now let's look at whether the first condition will be preserved. Operation I will preserve the condition for the winding of the paths being merged provided that we merge unpaired paths when possible. It will also satisfy the condition for the windings of the newly created paths since there are no $(-a, -b)$ paths. Operation II will preserve condition 1 for the windings of the paths being merged since it only deletes negatively oriented pairs. Figure 19 illustrates why Operation II creates negatively oriented pairs of opposite paths. For Operation III

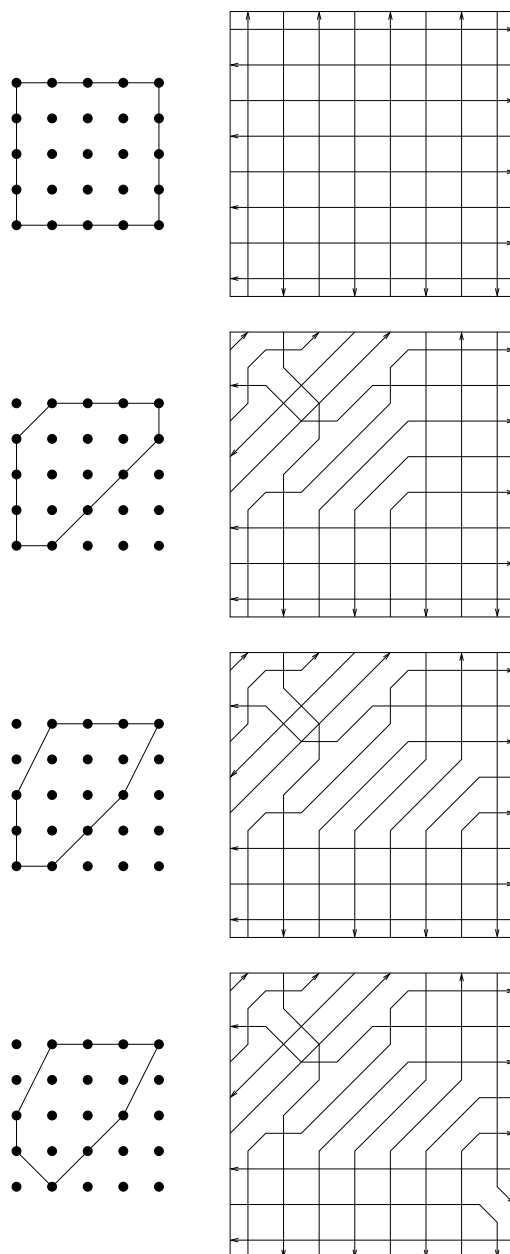


Figure 16: An example of the algorithm. Note that the cut made in the second diagram is the same as that of figure 12, although we have drawn it a little differently to make the spacings more equal.

we should again merge unpaired paths when possible. It is clear that the reinserted paths form pairs, and we can make these pairs negatively oriented if we desire.

Now consider whether extra crossings are introduced. Let the windings of the paths being merged be (a, b) , $(-a, -b)$, (c, d) , and $(-c, -d)$, where $ad - bc = 1$. A path of winding (e, f) will have extra crossings with the new $(a + c, b + d)$ paths if $af - be$ and $cf - de$ have opposite signs. Equivalently, there will be extra crossings if f/e is between b/a and d/c .

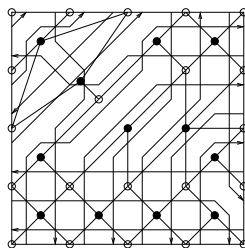
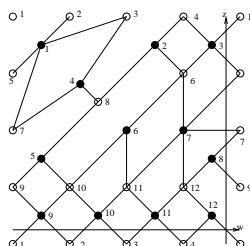


Figure 17: The dimer corresponding to the final zigzag path diagram in figure 16.



$$\begin{pmatrix}
 0 & 0 & z & 0 & 0 & 0 & 0 & 0 & -w & 0 & 0 & wz \\
 1 & 0 & 0 & 0 & 0 & 0 & 0 & 0 & w & -w & 0 & 0 \\
 1 & 0 & 0 & 1 & 0 & 0 & 0 & 0 & 0 & w & -w & 0 \\
 0 & 1 & 1 & 0 & 0 & 0 & 0 & 0 & 0 & 0 & w & -w \\
 -1 & 0 & z & 0 & 0 & 0 & z & 0 & 0 & 0 & 0 & 0 \\
 0 & 1 & -1 & 0 & 0 & 1 & 1 & 0 & 0 & 0 & 0 & 0 \\
 1 & 0 & 0 & -1 & 0 & 0 & z & z & 0 & 0 & 0 & 0 \\
 0 & -1 & 0 & 1 & 1 & 0 & 0 & 0 & 0 & 0 & 0 & 0 \\
 0 & 0 & 0 & 0 & -1 & 0 & 0 & z & 1 & 0 & 0 & 0 \\
 0 & 0 & 0 & 0 & 1 & -1 & 0 & 0 & 1 & 1 & 0 & 0 \\
 0 & 0 & 0 & 0 & 0 & 1 & -1 & 0 & 0 & 1 & 1 & 0 \\
 0 & 0 & 0 & 0 & 0 & 0 & 1 & -1 & 0 & 0 & 1 & 1
 \end{pmatrix}$$

$$\begin{aligned}
 \det = & (w^2 - w)z^4 + (-w^4 - 37w^3 - 137w^2 - 35w - 1)z^3 \\
 & + (3w^4 - 175w^3 + 146w^2 - 2w)z^2 \\
 & + (-3w^4 - 40w^3 - w^2)z + w^4
 \end{aligned}$$

Figure 18: The dimer corresponding to the final zigzag path diagram in figure 16 and its Kasteleyn matrix. The rows represent white nodes and the columns represent black nodes.

But because of the Farey fraction ordering, there are no windings (e, f) with this property. So extra crossings are not introduced.

Finally consider whether proper ordering is preserved. Again let the windings of the paths being merged be (a, b) , $(-a, -b)$, (c, d) , and $(-c, -d)$, $ad - bc = 1$. In Operation I, some nodes will see an (a, b) path or a (c, d) path become an $(a + c, b + d)$ path. Therefore proper ordering is preserved provided there are no windings between (a, b) and (c, d) . This is always the case because of the Farey fraction ordering. In Operation II, in addition to deletion we also need to move paths past each other. Some nodes are deleted and the others

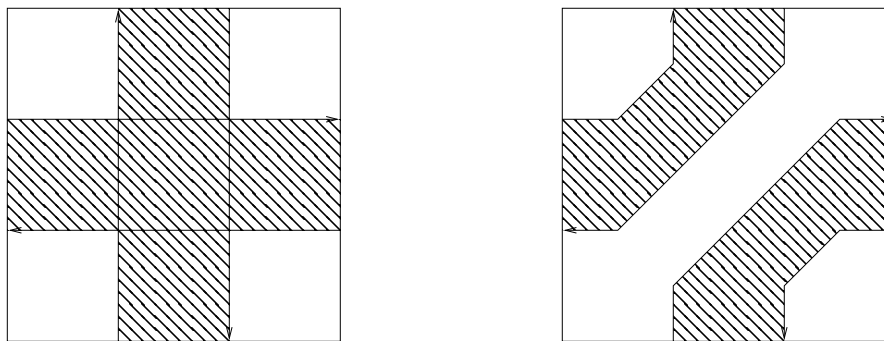


Figure 19: Left: We start out with two negatively oriented pairs of opposite paths. The shaded regions are free of crossings. Right: The regions formed by the merged pairs are still free of crossings.

remain unchanged, so proper ordering is preserved. In Operation III, the process of making the lone paths is the same as Operation I, so it preserves proper ordering. Removing pairs also preserves proper ordering. Inserting pairs of paths preserves proper ordering if each intersection between a path in the pair and another path has the same sign as their crossing number, i. e. the paths in the pair do not have extra crossings. Since we are inserting them along an existing path, they will not have extra crossings if the existing path does not have any. We have already showed that we never introduce extra crossings. \square

6.3 Allowing extra crossings

If we want to produce diagrams with extra crossings, we can always just skip the steps for removing the extra crossings. When we want to create (a, b) and $(-a, -b)$ paths, we just perform Operation I twice. There is one potential issue in that we have always assumed that the zigzag paths that we join have just one crossing. We always join paths with oriented crossing number ± 1 , but now the unoriented crossing number can be larger than the absolute value of the oriented number. But we recall that the only extra crossings we create are between paths with windings of the form (a, b) and $(-a, -b)$. We may later merge these paths with some other paths, but the extra crossings will always be between paths with oppositely signed x -coordinates and oppositely signed y -coordinates. We never merge such pairs of paths.

6.4 The number of independent solutions to the R -charge equations

We now exhibit the dimers required by Lemma 3.10.

Lemma 6.2. *The algorithm described in section 6.3 produces dimers for which the set of all solutions to equations (3.1) and (3.2) has dimension equal to the number of zigzag paths minus one.*

Proof. Our proof is by induction. Our algorithm starts with a dimer that is a diamond-shaped grid. We denote the position of an edge in the grid by (i, j) . We can see (e. g. by Fourier analysis) that the general solution to (3.1) and (3.2) is $\frac{1}{2} + (-1)^i f(j) + (-1)^j g(i)$ for arbitrary functions f, g . The number of independent solutions is the number of rows

plus the number of columns minus one (the minus one come from the fact that $f(j) = (-1)^j, g(i) = -(-1)^i$ produces the same solution as $f(j) = 0, g(i) = 0$), which is the number of zigzag paths minus one.

Now consider what happens when our algorithm deletes an edge of the toric diagram. If we have a solution to the equations (3.1) and (3.2) in the new dimer, we can construct a solution to the equations in the old dimer by assigning a value of zero to the deleted edge. Conversely, if we have a solution in the old dimer in which the deleted edge has value zero, then we have solution in the new dimer as well. We know that there exists a solution in the old dimer where the deleted edge is nonzero, since the deleted edge is contained in some boundary perfect matching. So deleting the edge reduces the dimension of the solution space of (3.1) and (3.2) by one, and also reduces the number of zigzag paths by one. \square

7. Conclusions

We showed that dimers that have the number of faces predicted by the AdS dual theory and that have valence one nodes will have many nice properties: they are “properly ordered”, their cubic anomalies are in agreement with the Chern-Simons coefficients of the AdS dual, gauge-invariant chiral primary operators satisfy the unitarity bound, corner perfect matchings are unique, and zigzag path windings are in one-to-one correspondence with the (p, q) -legs of the toric diagram.

We derived some simple bounds for the cubic anomaly a in terms of the area of the toric diagram (and hence in terms of the number of gauge groups).

We provided a precise, computationally feasible algorithm for producing a dimer model for a given toric diagram based on previous partial resolution techniques and the Fast Inverse Algorithm.

It would be interesting to see if our results could apply to the three-dimensional dimers discussed in [32] and the orientifold dimers discussed in [33].

Acknowledgments

I would like to thank Christopher Herzog for suggesting this problem to me and for providing many helpful discussions. I would like to thank Daniel Kane for helpful discussions regarding Lemmas 3.10 and 6.2 and Alberto Zaffaroni for discussion. I would also like to thank Amihay Hanany for introducing me to dimer models. This work was supported in part by the NSF Graduate Fellowship Program and NSF Grant PHY-075696.

References

- [1] J.M. Maldacena, *The large- N limit of superconformal field theories and supergravity*, *Adv. Theor. Math. Phys.* **2** (1998) 231 [*Int. J. Theor. Phys.* **38** (1999) 1113] [[hep-th/9711200](#)].
- [2] S.S. Gubser, I.R. Klebanov and A.M. Polyakov, *Gauge theory correlators from non-critical string theory*, *Phys. Lett. B* **428** (1998) 105 [[hep-th/9802109](#)].

- [3] E. Witten, *Anti-de Sitter space and holography*, *Adv. Theor. Math. Phys.* **2** (1998) 253 [[hep-th/9802150](#)].
- [4] P. Kasteleyn, *Graph theory and crystal physics*, in *Graph theory and theoretical physics*, F. Harary ed., Academic Press, London U.K. (1967).
- [5] A. Hanany and K.D. Kennaway, *Dimer models and toric diagrams*, [hep-th/0503149](#).
- [6] S. Franco, A. Hanany, K.D. Kennaway, D. Vegh and B. Wecht, *Brane dimers and quiver gauge theories*, *JHEP* **01** (2006) 096 [[hep-th/0504110](#)].
- [7] S. Franco et al., *Gauge theories from toric geometry and brane tilings*, *JHEP* **01** (2006) 128 [[hep-th/0505211](#)].
- [8] A. Hanany and D. Vegh, *Quivers, tilings, branes and rhombi*, *JHEP* **10** (2007) 029 [[hep-th/0511063](#)].
- [9] B. Feng, Y.-H. He, K.D. Kennaway and C. Vafa, *Dimer models from mirror symmetry and quivering amoebae*, [hep-th/0511287](#).
- [10] J. Stienstra, *Hypergeometric systems in two variables, quivers, dimers and dessins d'enfants*, [arXiv:0711.0464](#).
- [11] M.R. Douglas, B.R. Greene and D.R. Morrison, *Orbifold resolution by D-branes*, *Nucl. Phys.* **B 506** (1997) 84 [[hep-th/9704151](#)].
- [12] D.R. Morrison and M.R. Plesser, *Non-spherical horizons. I*, *Adv. Theor. Math. Phys.* **3** (1999) 1 [[hep-th/9810201](#)].
- [13] B. Feng, A. Hanany and Y.-H. He, *D-brane gauge theories from toric singularities and toric duality*, *Nucl. Phys.* **B 595** (2001) 165 [[hep-th/0003085](#)].
- [14] I. Garcia-Etxebarria, F. Saad and A.M. Uranga, *Quiver gauge theories at resolved and deformed singularities using dimers*, *JHEP* **06** (2006) 055 [[hep-th/0603108](#)].
- [15] S. Benvenuti, L.A. Pando Zayas and Y. Tachikawa, *Triangle anomalies from Einstein manifolds*, *Adv. Theor. Math. Phys.* **10** (2006) 395 [[hep-th/0601054](#)].
- [16] G. Mack, *All unitary ray representations of the conformal group $SU(2,2)$ with positive energy*, *Commun. Math. Phys.* **55** (1977) 1.
- [17] V.K. Dobrev and V.B. Petkova, *All positive energy unitary irreducible representations of extended conformal supersymmetry*, *Phys. Lett.* **B 162** (1985) 127.
- [18] S. Benvenuti, S. Franco, A. Hanany, D. Martelli and J. Sparks, *An infinite family of superconformal quiver gauge theories with Sasaki-Einstein duals*, *JHEP* **06** (2005) 064 [[hep-th/0411264](#)].
- [19] W. Fulton, *Introduction to toric varieties*, Princeton University Press, Princeton U.S.A. (1993).
- [20] A. Butti and A. Zaffaroni, *R-charges from toric diagrams and the equivalence of a -maximization and Z -minimization*, *JHEP* **11** (2005) 019 [[hep-th/0506232](#)].
- [21] K.A. Intriligator and B. Wecht, *The exact superconformal R-symmetry maximizes a* , *Nucl. Phys.* **B 667** (2003) 183 [[hep-th/0304128](#)].
- [22] S. Lee and S.-J. Rey, *Comments on anomalies and charges of toric-quiver duals*, *JHEP* **03** (2006) 068 [[hep-th/0601223](#)].

- [23] A. Kato, *Zonotopes and four-dimensional superconformal field theories*, *JHEP* **06** (2007) 037 [[hep-th/0610266](#)].
- [24] D. Martelli, J. Sparks and S.-T. Yau, *The geometric dual of α -maximisation for toric Sasaki-Einstein manifolds*, *Commun. Math. Phys.* **268** (2006) 39 [[hep-th/0503183](#)].
- [25] W. Blaschke, *Über Affine Geometrie VII: Neue Extremeigenschaften von Ellipse und Ellipsoid*, *Ber. Verh. Sachs. Akad. Wiss. Leipzig Math.-Phys. Kl.* **69** (1917) 306.
- [26] C.M. Petty, *Affine isoperimetric problems*, *Ann. N. Y. Acad. Sci.* **440** (1985) 113.
- [27] B.V. Karpov and N. D. Yu, *Three-block exceptional collections over del Pezzo surfaces*, *Izv. Ross. Akad. Nauk Ser. Mat.* **62** (1998) 429 [[alg-geom/9703027](#)].
- [28] S.S. Gubser, *Einstein manifolds and conformal field theories*, *Phys. Rev. D* **59** (1999) 025006 [[hep-th/9807164](#)].
- [29] M. Henningson and K. Skenderis, *The holographic Weyl anomaly*, *JHEP* **07** (1998) 023 [[hep-th/9806087](#)].
- [30] A. Bergman and C.P. Herzog, *The volume of some non-spherical horizons and the AdS/CFT correspondence*, *JHEP* **01** (2002) 030 [[hep-th/0108020](#)].
- [31] B. Feng, S. Franco, A. Hanany and Y.-H. He, *Symmetries of toric duality*, *JHEP* **12** (2002) 076 [[hep-th/0205144](#)].
- [32] S. Lee, *Superconformal field theories from crystal lattices*, *Phys. Rev. D* **75** (2007) 101901 [[hep-th/0610204](#)].
- [33] S. Franco et al., *Dimers and Orientifolds*, *JHEP* **09** (2007) 075 [[arXiv:0707.0298](#)].